Submitted for Publication to SOLAR ENERGY

PRODUCING SATELLITE-DERIVED IRRADIANCES IN COMPLEX ARID TERRAIN

Richard Perez
ASRC, the University at Albany
251 Fuller Rd.
Albany, NY 12203
perez@asrc.cestm.albany.edu

Pierre Ineichen,
CUEPE, University of Geneva
7 Route de Drize
1227 Carouge, Switzerland
Pierre.Ineichen@cuepe.unige.ch

Marek Kmiecik, ASRC
Kathleen Moore, IED
251 Fuller Rd.
Albany, NY 12203
moore@iedat.com

David Renne & Ray George
NREL
1617 Cole Blvd.
Golden, CO 80401
drenne / ray_george@nrel.nrel.gov

ABSTRACT

This paper describes a methodology to correct satellite-derived irradiances over complex terrain for models that use the visible satellite channel as main input for cloud index determination. Complex terrain is characterized by high reflectance surface and or the juxtaposition of high and low reflectance surfaces (e.g., desert plains and forested ridges). The correction consists of (1) climate dependent post-model clear sky calibration and (2) singularity identification and removal.

1. DESCRIPTION OF CURRENT MODEL

The authors recently proposed a new semi-empirical model for deriving global and direct irradiances from the visible channel[1] of geostationary weather satellites (Perez et al., 2002). This model was a logical evolution of earlier work by Cano et al., (1986) and Zelenka et al., (1999).

---

[1] *Weather satellites typically have several sensors monitoring the earth in different spectral bands. The "visible channel" records wavelengths in the visible spectral range (0.55-0.75 μm) corresponding to the peak of the solar radiation spectrum.*

In its simplest description the model amounts to the modulation of clear sky -- global and direct -- envelopes as a function of satellite-derived **cloud indices**. The clear sky envelopes are locally adjustable for regional/seasonal turbidity and ground elevation.

For a given time/location, a cloud index is derived from image's pixel brightness in relation to the local pixel's **dynamic range** -- i.e., the possible range of pixel brightness at the considered location, with the darkest pixels corresponding to clear conditions and the brightest to cloudy conditions. Pixel dynamic range varies as a function of location and time because of ground reflectivity (albedo), ground bi-directional – specular – reflectivity, the presence of snow cover, and the satellite sensor's calibration. In its operational version, the model maintains individual, unique dynamic ranges for all locations. Dynamic ranges evolve over time and are derived from the flux of incoming pixel counts at each location (see Fig. 1). This approach allows the model to dispense with absolute satellite calibration (Perez et al., 2002) and to account for seasonal and geographical changes in ground reflectivity. Further, access to external information on ground snow cover (Perez et al., 2002) allows the model to also account for snow in its dynamic range management.

Ground specular reflectance had been identified as the main source of model inaccuracy in arid regions. The model addresses the bi-directional reflectance issue by deriving daily/seasonal specular reflectance signatures for each individual location. These signatures are based upon the history of pixel brightness at each considered location, by looking at the variation of observed dynamic ranges' lower bound as a function of day-of-year and time of day (Perez et al., 2002).

2. LIMITATIONS OF CURRENT MODEL IN COMPLEX AND/OR ARID TERRAIN

The model was tested against ground truth stations located in the arid western US and was found to perform adequately (Perez et al., 2002). However, these stations, namely, Daggett, CA, Albuquerque, NM and Burns, OR, are not located in extreme ground reflectance environments.

We define extreme ground reflectance environments as

(1) very high specularity regions such as salt beds found throughout the southwestern US and Mexico and in many other arid regions of the world, and/or
(2) the juxtaposition of bright and dark areas, such as arid plains and forested ridges (see Fig.2)

In the first case, the specular signature imbedded in the current model proved to be sometimes insufficient, leading to small but significant underestimations, particularly noticeable on the direct irradiance (DNI) component. In the second case, slight satellite navigation uncertainties may induce very large errors. Indeed, because location-specific dynamic ranges are maintained by the flux of incoming pixel counts at that location, a satellite navigation error may at times "throw in" dark pixels (from a forested ridge) into otherwise bright ground regions. These few dark pixels reduce the local dynamic range's lower bound, resulting in large model underestimation, because most clear occurrences are mistaken for cloudy conditions when contrasting the clear bright ground pixel against the darker dynamic range. This process is illustrated in Fig. 3.

3. PROPOSED SOLUTION

We developed a two-step addition to the model in an attempt to address these shortcomings.

Step-1: Clear sky calibration

By definition, the lower bound of the dynamic range corresponds to viewing, through a clear sky, a pixel illuminated by clear sky global (GHI) and direct (DNI) irradiances. At some locations, this clear sky limit may not be achieved by the model, because of an underestimated specular signature, or because of the contamination of the lower bound by neighboring darker pixels. In the first case the limit may be reached only at some hours in the day. In the second case, the limit may not be reached at all. In order to force the model to reach this limit, we postulate that for each monthly period, GHI and DNI are bound to reach their clear sky limit at least "n" times for each daylight hour. The value of "n" may be adjusted to reflect prevailing regional insolation conditions. For very clear/arid regions in the SW US, a value in the 5-10 range -- out of 28 to 31 days in a month -- was found to be conservative. This assumption allows us to derive a set of correction coefficients for

each pixel, each time-of-day and each month, defined as the ratio between the clear sky (DNI or GHI) value and the n^{th} highest achieved value for each hour in the considered monthly period, and thus to produce a calibrated time series.

Step-2; Removal of singularities

Even after application of the above correction, we found that there remained micro regions of model underestimation. We believe that in these small, highly reflective regions, the model approaches its clear sky limit often enough, because of mis-navigated neighboring darker pixels, so that the clear sky calibration correction is underestimated. These micro-regions errors become visible as singularities when average DNI values are mapped (see Fig. 4). Our approach for this second step correction is to use the average maps themselves as the instrument of data correction. For both the DNI and GHI components, the corrective process scans the monthly average maps in latitude and longitude to detect pixel-to-pixel irradiance variation. If a threshold -- currently set at 2.5% for monthly average DNI and 1.5% for GHI for two neighboring locations (distant of 10 km) -- is exceeded, the model reduces the singularity by returning an average of the neighboring pixels. In this process, a monthly averaged map without singularities (fig. 4) is constructed. If necessary, time series at the corrected locations may be generated using a secondary model previously developed by the authors (Perez, 2001). This secondary model is designed to simulate a time series of global and direct irradiance from the knowledge of (1) an existing time series – in the present case the uncorrected time series – and (2) the monthly average modified clearness index (Perez et al, 1990) difference between the uncorrected and the corrected monthly maps.

4. DISCUSSION

We have presented a robust, straightforward two-step approach to correct irradiance estimated from weather satellites' visible channel, in cases where terrain reflectivity and texture limit the model ability to perform reliably. The first step – clear sky calibration – typically results in correction of less than 5% for global and less than 10% for direct in bright terrain conditions. The second step may result in higher corrections, but only for a very limited number of pixel locations.

As an alternate approach we are exploring using the IR channel in addition to the visible channel in these difficult locations.

Validation: the initial model had been thoroughly validated for several climatically distinct locations (Perez et al., 2002). Additional validations for this proposed model update are not as straightforward to accomplish, because few ground-truth stations are deployed in problematic micro-regions. However, the NOAA-SURFRAD station of Desert Rock, NV (SUFRAD, 2003) happens to be located in an arid valley with high ground reflectivity and could be used to test the first step of the proposed model modification. Validation results are shown in Fig. 5. They clearly show that the clear-sky calibration brings modeled values much closer to the 1-1 line. The yearly MBEs prior to correction were respectively -4% for global and -11% for direct. After correction, both MBEs are within 1%.

No station was found to operate in micro-structure areas where the step-2 modification would be necessary. However it should be noted, at the very least, the implementation of step-2 provides a means of assessing data quality by gauging the magnitude of the correction applied to any given pixel.

5. ACKNOWLEDGEMENT

This paper is a by-product of research and development efforts funded by the USDOE via University of Oregon (280111A), NREL (DE-AC36-99GO10337 and AXE-0-30070-01) and UNEP (SWERA GF/2721-01-4378).

6. REFERENCES

(1) Perez R., P. Ineichen, K. Moore, M. Kmiecik, C. Chain, R. George and F. Vignola, (2002): A new operational model for satellite-derived irradiances description and validation. Solar Energy (in press).
(2) Cano, D., J.M. Monget, M. Aubuisson, H. Guillard, N. Regas and L. Wald, (1986): A Method for the Determination of Global Solar Radiation from Meteorological Satellite Data. Solar Energy 37, pp. 31-39

(3) Zelenka, A., Perez R, Seals R. and Renné D., (1999): Effective Accuracy of Satellite-derived irradiance, Theoretical and Applied Climatology, 62, 199-207
(4) Perez, (2001): A time Series Generator. Technical Report No. 3. NREL contract AXE-0-30070-01. NREL, Golden, CO.
(5) Perez, R., P. Ineichen, R. Seals and A. Zelenka, (1990): Making Full Use of the Clearness Index for Parameterizing Hourly Insolation Conditions. Solar Energy 45, pp. 111-1
(6) The SURFRAD Network -- Monitoring Surface Radiation in the Continental United States. NOAA, Surface Radiation Research Branch (http://www.srrb.noaa.gov/surfrad/index.html)

Figure titles

Fig 1: Evolution of dynamic range at a sample location. Each dot represents a pixel count corrected for solar incidence. The upper bound reflects the decay of satellite calibration. The lower bound reflects seasonal variability of ground albedo. Both upper and lower bounds are derived from the history of pixel count at that location.

Fig. 2: Satellite view of the southwest US showing complex ground reflectivity. Two extreme cases – salt beds – are shown by arrows. One of these salt beds is shown on the right as seen from an airplane at 10 km elevation.

Fig. 3: Illustration of dynamic ranges for two neighboring pixels near Death-Valley, California. One of the pixels (A) has a dark albedo and the other (B) a high ground albedo (see satellite scene top left). Routine satellite navigation uncertainties result in an artificial decrease of the apparent pixel B's lower bound, because pixel A values are sometime recorded in pixel B location. As a consequence, pixel B appears considerably cloudier than pixel A, leading to irradiance underestimation at that location.

Fig. 4: Comparing uncorrected and corrected (both step-1 and step-2) monthly averaged direct irradiance maps in a 400 x 400 km region straddling California and Nevada (average Wm^{-2}). Note that the overall upper trend is largely due to implementation of step-1, while the elimination of singularities is a result of step-2.

Fig. 5: Satellite estimated vs. ground truth measurements at Desert Rock, NV, for global irradiance before and after step-1 correction (respectively A and B) and direct irradiance before and after step-1 correction (respectively C and D)

FIGURE 1

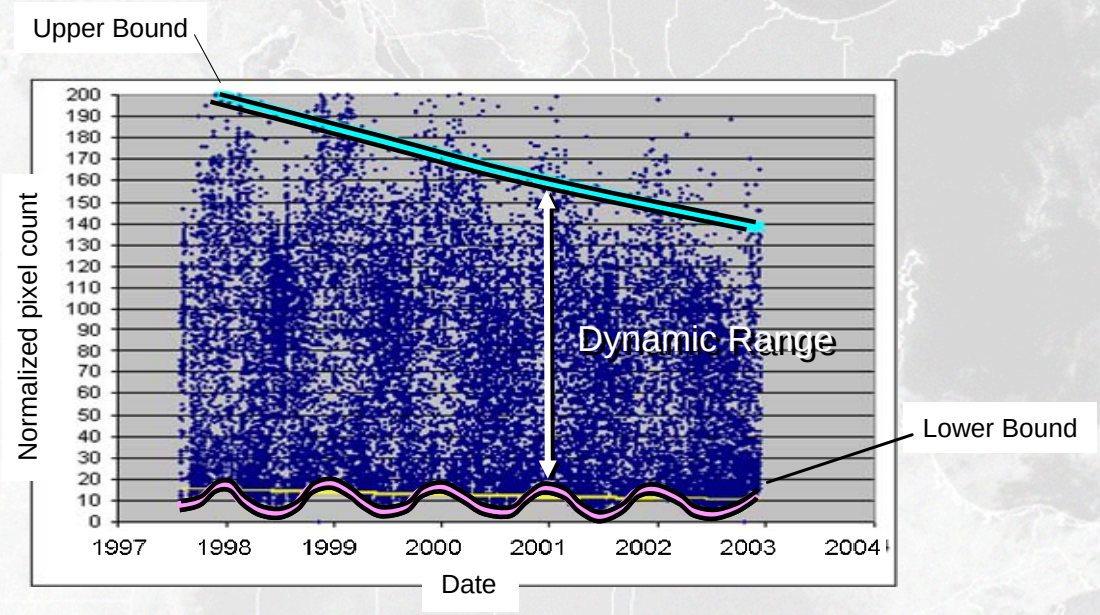
Upper Bound
Normalized pixel count
200
190
180
170
160
150
140
130
120
110
100
90
80
70
60
50
40
30
20
10
0
1997
1998
1999
2000
2001
2002
2003
2004
Date
Dynamic Range
Lower Bound

FIGURE 2

FIGURE 3

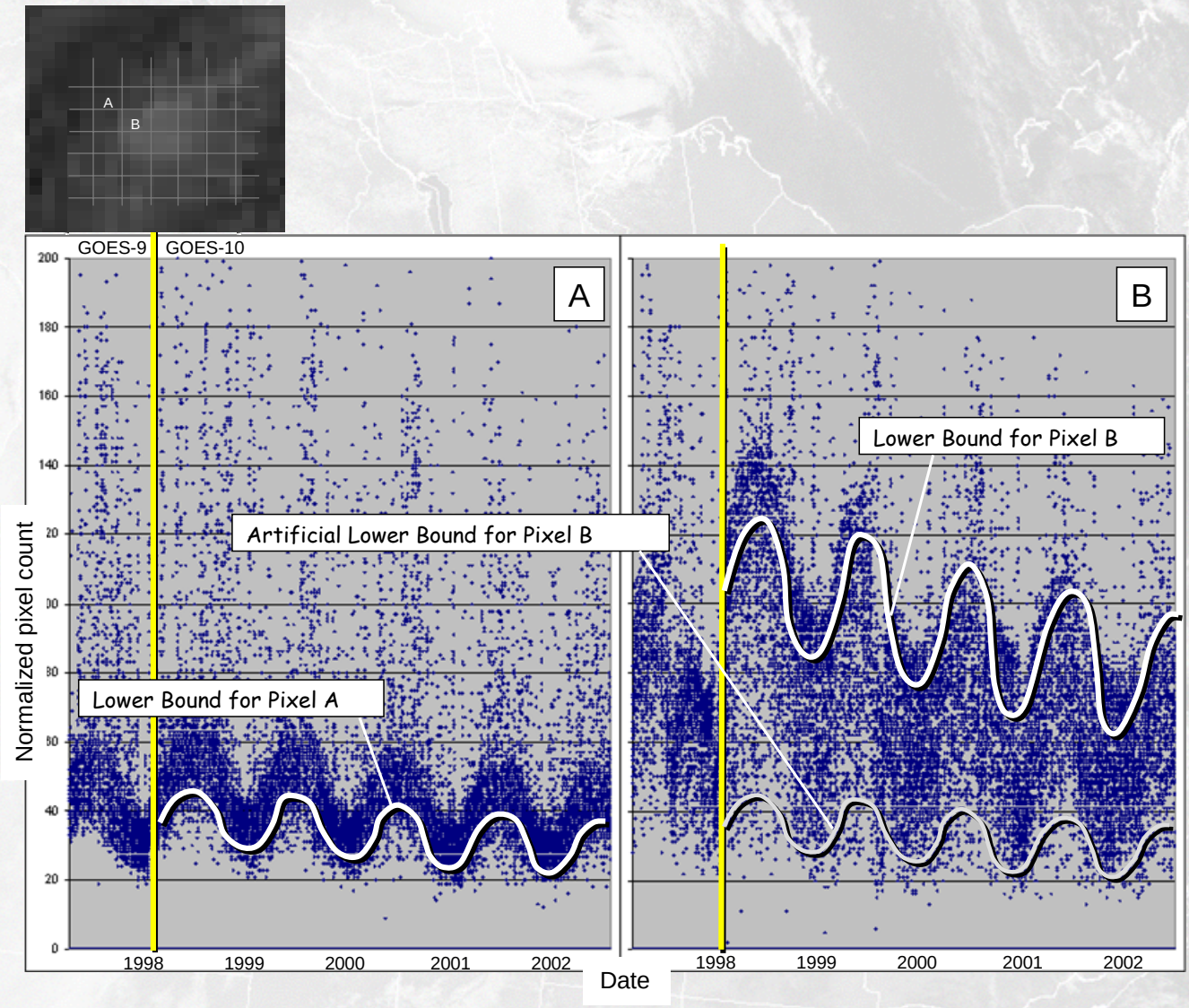
A
B
GOES-9
GOES-10
A
B
Lower Bound for Pixel B
Artificial Lower Bound for Pixel B
Lower Bound for Pixel A
Normalized pixel count
200
180
160
140
120
100
80
60
40
20
0
1998
1999
2000
2001
2002
Date

FIGURE 4

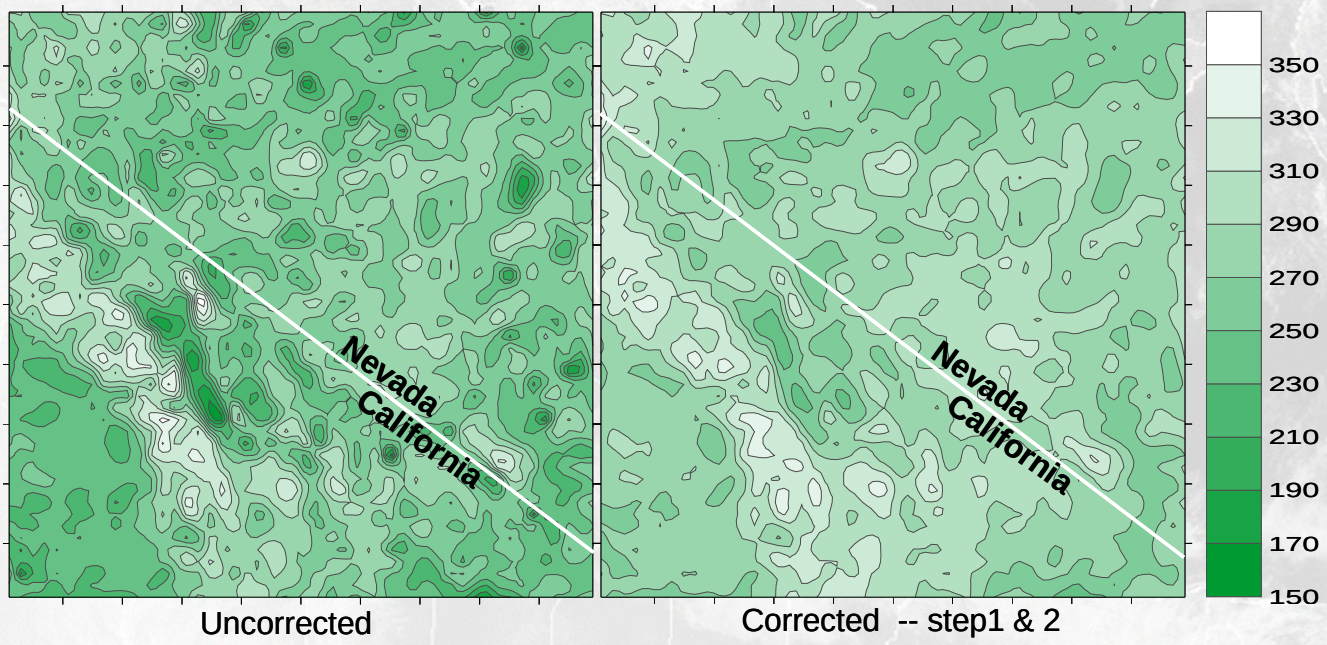
Nevada
California
Uncorrected
Nevada
California
Corrected -- step1 & 2
350
330
310
290
270
250
230
210
190
170
150

FIGURE 5

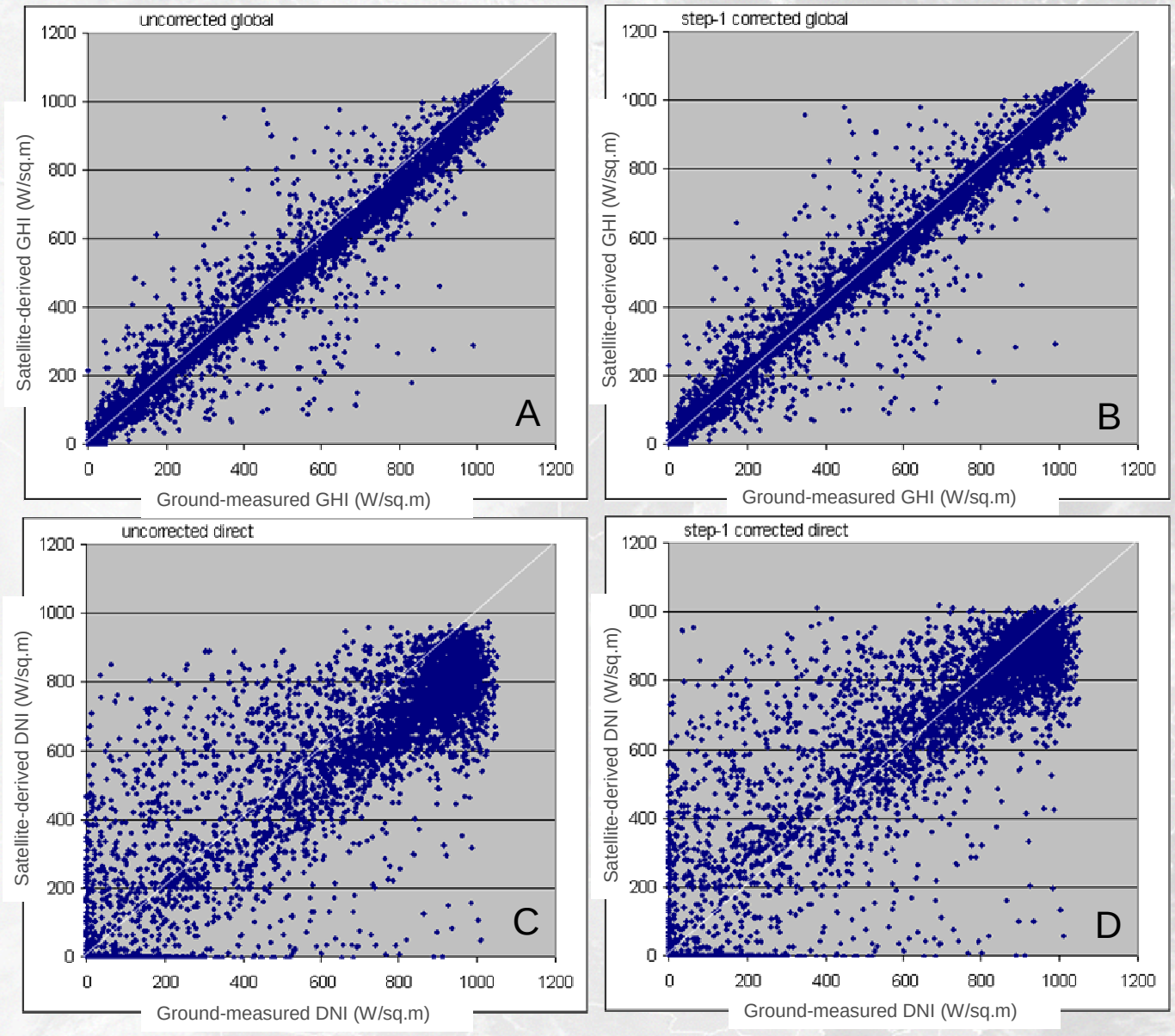
uncorrected global
Satellite-derived GHI (W/sq.m)
Ground-measured GHI (W/sq.m)
A
step-1 corrected global
Satellite-derived GHI (W/sq.m)
Ground-measured GHI (W/sq.m)
B
uncorrected direct
Satellite-derived DNI (W/sq.m)
Ground-measured DNI (W/sq.m)
C
step-1 corrected direct
Satellite-derived DNI (W/sq.m)
Ground-measured DNI (W/sq.m)
D
0
200
400
600
800
1000
1200